Int. J. Heat Mass Transfer. Vol. 32, No. 6, pp. 1077–1093, 1989
Printed in Great Britain

0017–9310/89 $3.00+0.00

An experimental study of vapour growth at the superheat limit temperature

H. McCANN, L. J. CLARKE and A. P. MASTERS
Shell Research Ltd., Thornton Research Centre, P.O. Box 1, Chester CH1 3SH, U.K.

(*Received* 20 *June* 1988 *and in final form* 26 *October* 1988)

Abstract—The vaporization of liquid n-butane at its superheat limit temperature is filmed at speeds of up to 5×10^5 frames per second and the associated far-field pressure is studied. Bubble growth rates of up to 25 m s^{-1} are measured and compared with theoretical models and previous experimental data. The far-field pressure is distorted by multiple reflections within the butane droplet, although this does not explain all the structure in the first 13 μs or so of the recorded pressures; in particular, bubble growth becomes very dramatic after about 7 μs. Various other details of the pressure traces can be understood in terms of bubble behaviour.

INTRODUCTION

RAPID vaporization of a cold, volatile liquid, when brought into contact with a much hotter, stable liquid, is a well-known hazard in several industries, such as metal melting, paper making, nuclear power generation and liquefied natural gas production. The explosive nature of these interactions implies that the phenomenon is due to rapid mass transfer from the liquid phase to the vapour phase. In this respect, the phenomenon of vaporization at the superheat limit temperature, T_{SL}, is thought to be of fundamental importance in several of the liquid–liquid systems encountered in the above industries [1].

In the absence of external nucleation centres, a liquid can be heated to temperatures far above its boiling point, ultimately undergoing spontaneous homogeneous nucleation of vapour at its superheat limit temperature. For many light hydrocarbons, T_{SL} is about $0.9T_c$ (see, for example, the reviews by Blander and Katz [2] and Avedisian [3]) and the stored thermal energy in the liquid phase prior to vaporization is thus considerable. Vapour bubble growth after nucleation at T_{SL} has received some experimental attention in recent years [4–7]. Shepherd and Sturtevant [4] have shown that bubble growth and mass transfer at T_{SL} can be much more rapid than at low superheats and indeed, more rapid than would be expected from low superheat models, such as that due to Prosperetti and Plesset [8], when extrapolated to T_{SL}. Shepherd and Sturtevant attributed this to the observed roughening of the vapour–liquid interface, which they ascribed to a mechanism originally proposed by Landau [9] concerning flame stability. The stability of an evaporating interface has since been studied by Prosperetti and Plesset [10] and by Higuera [11], who found that instabilities are indeed to be expected over a large range of wave numbers, particularly when the evaporation mass flux is large. Avedisian [5] reported that the rapid bubble growth could be suppressed by applying a high ambient pressure to the system and this was shown by Frost and Sturtevant [6] to be due to suppression of the instability at the liquid–vapour interface. This discovery enabled further study of the phenomenon both before and after the onset of instability [6, 7] and, in particular, Frost [7, 15] has demonstrated that the instability roughening of the interface induces a two-phase mass transfer, as speculated by Shepherd and Sturtevant.

A theoretical model has been developed at Thornton Research Centre by Nguyen *et al.* [12] (referred to as 'the TRC model'), with the aim of understanding the rate of bubble growth and generation of far-field pressure after the interface had been roughened by the instability. This model incorporates fluid dynamical effects and two-phase mass transfer, leading to higher rates of mass transfer than predicted by the model of Prosperetti and Plesset [8] (hereafter referred to as 'the classical theory'). Thus the TRC model predicts a rate of far-field pressure generation which is orders of magnitude larger than that predicted by the classical theory.

This paper reports results of an experimental programme at TRC which was aimed specifically at testing the TRC model.

OVERVIEW OF EXPERIMENTAL TECHNIQUE

The technique adopted to superheat the droplet is that of Moore [13], which has been widely used. It consists of introducing a droplet of the test liquid into a host liquid in which the test liquid is buoyant and immiscible. The host liquid is in a vertical column and is differentially heated so that it is below the test liquid's boiling point at the bottom, but above the superheat limit temperature of the test liquid at the top. Vaporization occurs within a few millimetres of

NOMENCLATURE

c	speed of sound
D	droplet diameter
J_0	rate of production of super-critical nucleation centres per cm^3 per second at a reference temperature
$J(T)$	rate of production of super-critical nucleation centres per cm^3 per second at any given temperature
L	parameter in expression for $J(T)$
N_0	number of droplets at a reference temperature
$N(T)$	number of droplets at any given temperature
$p(t)$	observed pressure at any given time
$q(t)$	primordial pressure at any given time
r	bubble radius
R_0	pressure reflection coefficient for a pulse incident from liquid butane on an interface with butane vapour
R_D	pressure reflection coefficient for a pulse incident from liquid butane on an interface with ethylene glycol
$s(t)$	resultant pressure at any given time, calculated from the reverberation model
t	time
T	temperature
T_c	critical temperature
T_{SL}	superheat limit temperature
T_D	pressure transmission coefficient for a pulse incident from liquid butane on an interface with ethylene glycol
T_i	constant time values in reverberation model
u	bubble growth velocity
V	droplet volume
$\langle x \rangle$	average value of any variable x.

Greek symbols

δ_1	time from nucleation to the first bump in the pressure trace
δ_{ij}	time between bumps in pressure trace.

the centre of a cubic observation chamber of side 12 cm. The basic apparatus is shown in Fig. 1.

The test liquid chosen for the present study was n-butane, which, at atmospheric pressure, has a boiling point of -0.5°C and a superheat limit temperature of 105°C [2, 3]. The host liquid was ethylene glycol. The temperature profile of the column was chosen so as to keep the heating rate of the test liquid droplets constant until they were within about 4 cm of the location of T_{SL}, where a higher temperature gradient (1.2°C cm^{-1}) was imposed in order to localize the nucleation point in space as accurately as possible. In most of the experiments discussed here, droplets of a diameter of 1.35 mm were used, the spread in diameter being only 0.025 mm (standard deviation). This droplet size will be assumed in all discussions below unless explicitly noted otherwise. The droplets were injected into the column with a hypodermic syringe needle of 0.10 mm i.d. and 0.23 mm o.d. Adapting a solution to the heat transfer problem which was put forward by Skripov [14], the under-heating of the droplet centre compared with the edge is expected to be of the order of 4°C when the edge is at T_{SL}. In fact this calculation neglects any mixing effects in the droplet, so it is very much an upper limit to the temperature difference. In some cases, droplets of diameter 1.77 mm were used, by employing a larger syringe needle.

The probability of spontaneous homogeneous nucleation as a function of temperature was calculated from the following expression due to Blander and Katz [2]:

$$N(T) = N_0 \exp\left\{-\frac{VJ(T)}{L(\mathrm{d}T/\mathrm{d}t)}\right\} \tag{1}$$

where

$$J(T) = J_0 \exp\{LT\} \tag{2}$$

and L is taken to be 7°C^{-1}. It was found to have a full width at half maximum height (FWHM) of 0.34°C for the relevant experimental parameters, assuming perfect temperature stability in the column. Expressing the probability density as a function of time with respect to the time at which the droplet passed a fixed point in the column a few centimetres below the nucleation region, the FWHM in the time distribution is 32 ms. Temperature instability in the apparatus worsens this to about 38 ms. This was tested by having the droplets rise through a laser beam to start a clock which was then stopped by detecting the pressure pulse from the exploding droplets. The theoretical and experimental distributions of nucleation time were in good agreement. This is good evidence that nucleation is indeed homogeneous. The width of the distribution implies that photographic observation of the first 100 μs or so of the bubble growth process has to be initiated ('triggered') after nucleation has taken place, and a reasonably large field of view, about 4 or 5 mm high, has to be filmed.

The recording equipment was triggered by a pulse from a pressure transducer mounted close to the evaporating droplet. The trigger circuit and overall data acquisition system are shown in Fig. 2. Two

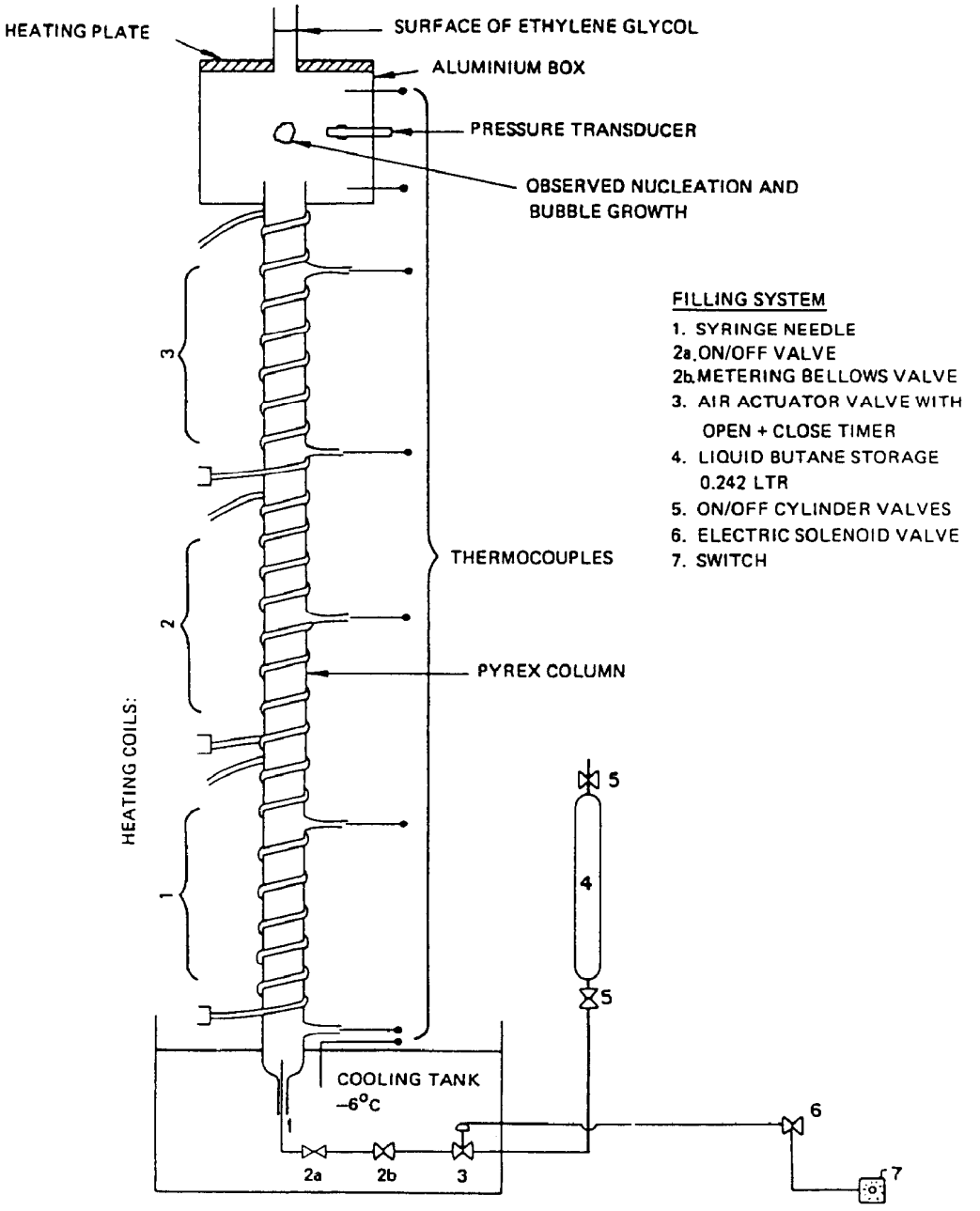

FIG. 1. Schematic diagram of the apparatus for raising liquid butane droplets to their superheat limit temperature.

different types of transducer were used for triggering: a Kistler 603B, which has a rise time of less than 1 μs, and a B&K 8103, which has a rise time of 7.5 μs. The trigger threshold corresponded to an over-pressure of about 3 mbar at the transducer, which was typically 2 or 3 mm from the exploding droplet when very early photographs were required, and about 10 mm otherwise.

A Hadland IMACON 790 image-convertor camera was used to film the vapour growth at speeds of 10^5 and 5×10^5 frames per second (fps). The optical system and the camera combined to give an overall magnification of 3.5×, and the actual field of view was 5.1×4.7 mm^2. After triggering, the camera delay to the first frame is about half of the inter-frame time; it is accurately calibrated by the manufacturers. Eight frames were recorded for each exploding droplet, on a single 5 × 4 in. film plate which was held in contact with the fibre optic output from the camera.

Illumination of the subject is a major limitation in this experiment. Firstly, it is necessary to illuminate the subject rapidly after the trigger is formed. Then a very intense flash of long duration is required and the light has to be diffuse [4]. It is also desirable that the

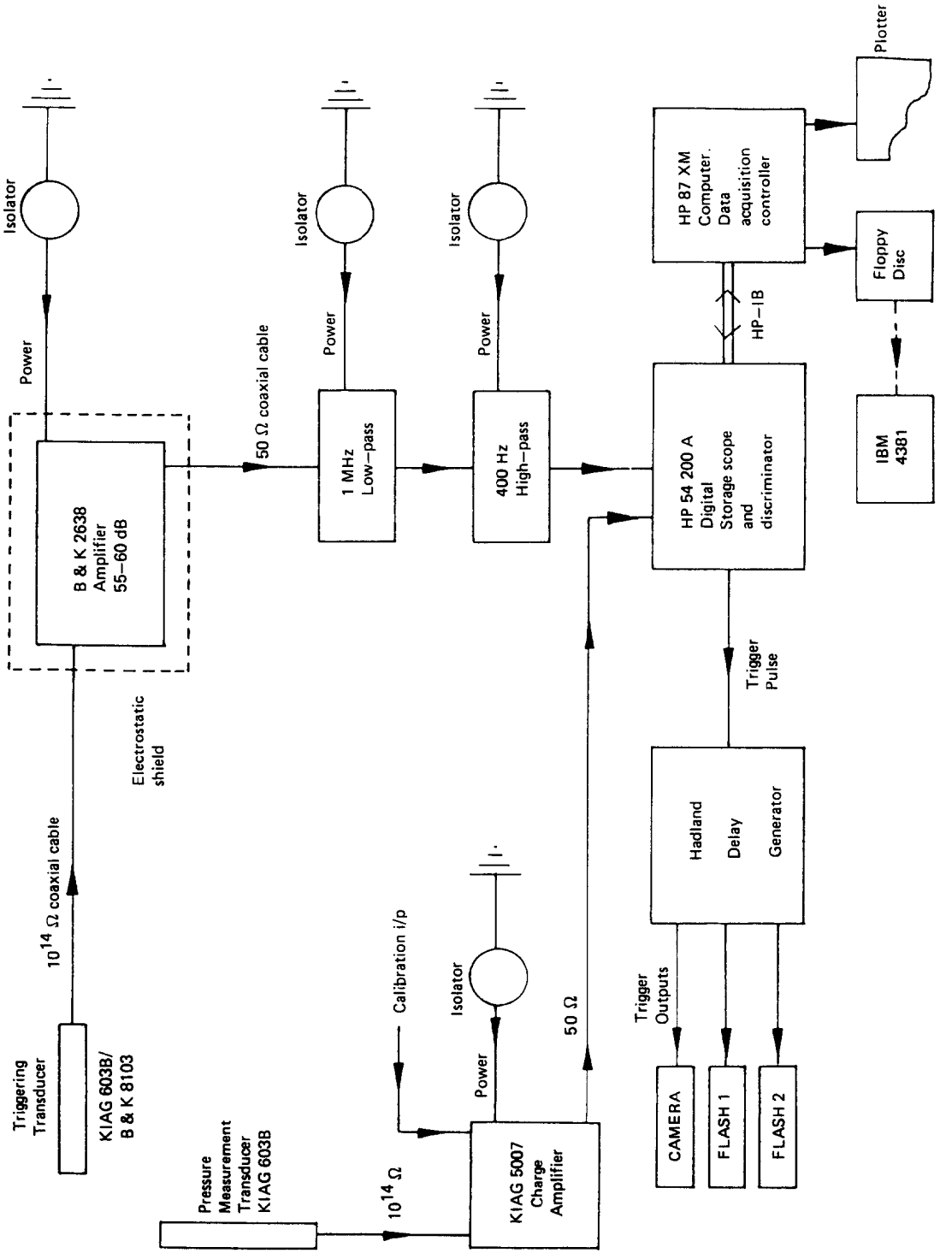

FIG. 2. Schematic diagram of the trigger and pressure measurement circuits and subsequent data flow.

flash does not generate spurious transducer signals by r.f. pick-up, etc. No single flash system was able to fulfil all of these conditions, and so the flash system had to be modified to acquire different types of photographic and acoustic data. In most cases, illumination of the subject was at about 90° to the lens axis ('side-lighting'), so large lens apertures (typically f5.6) had to be used, thus reducing the optical depth of focus. Calibrated pressure traces were obtained from a Kistler 603B transducer connected to a Kistler 5007 charge amplifier. The transducer has a natural frequency greater than 400 kHz and the charge amplifier filters out frequencies greater than 330 kHz.

BUBBLE GROWTH

General

The first frame of each film sequence in this experiment was obtained between 4 and 16 μs after nucleation, depending on the details of the hardware and the position of nucleation within the droplet. Analysis to date has concentrated on data obtained with the Hadland 20/50 flash unit, which gives a 20 or 50 μs flash duration with a rise time of about 4 μs. Data were obtained at both 10^5 and 5×10^5 fps, but the analysis presented here concentrates on the slower framing rate for reasons to be discussed below.

Figure 3 shows an example of data collected at 10^5 fps with the 20/50 illumination. The background is dark, as is the interior of the butane droplet. The two-dimensional projection of the droplet can be seen due to specular reflection at its smooth interface with the glycol host. The entire butane vapour region appears white due to reflection and refraction at its rough interface with both the butane and glycol. In this particular case, the first frame was obtained 13 μs after nucleation. The 603B transducer was very close to the droplet, and it can be seen as a vertical stripe of white light in the photographs. All times quoted below for photographs and other observations are understood to be relative to the time of vapour nucleation, unless otherwise indicated. In the case of photographs, allowance has been made for the transit time of the pressure pulse through the liquid butane and the glycol host and all electronic delays in the system. The error on the quoted time of each photograph is less than 0.5 μs.

Generally, the nucleation site can be anywhere in the droplet in three dimensions, although it tends to be near to the surface and its location is marked by the position of the characteristic 'cap' which is clearly illustrated in Fig. 3. It is clear from analysis of several droplets that vapour growth takes place in the direction away from the cap, towards the centre of the droplet; this defines the 'growth plane'. Therefore, it is only interesting to measure vapour growth in those cases where the growth plane is parallel to the film plane; this plane is called the 'optimum growth plane'. It has been previously demonstrated [6, 7, 15] that the cap is formed by the surface of the vapour bubble after it has reached the droplet edge and that, before that time, the entire bubble surface is smooth. In the present experiment, the cap is observed to be smooth in photographs taken at 5×10^5 fps where the first frame is obtained at about 7 μs. The cap is then observed to roughen in subsequent frames and become completely white at about 13 μs.

The rough interface between the butane liquid and its vapour can be clearly seen in these photographs. Visual examination reveals that the small-scale roughening occurs with a characteristic length of the order of 30 μm. Larger scale roughening is only clearly visible where the vapour–liquid interface lies close to the film plane; it has a characteristic length of the order of 200 μm. Quantitative analysis of these features is still in progress. It is worthwhile to note that, although side-lighting suffers from the drawback of yielding only low light levels, as noted earlier, it nonetheless provides a 'clean' view of the interface, with light which is reflected or refracted only once. This is to be compared with back-lighting, where the light is refracted twice by the rough interface. In principle, therefore, side-lighting yields a higher-fidelity view of the surface texture. Sturtevant and co-workers have attributed the small-scale roughening to the Landau instability. Furthermore, they attribute the concentric ring structure around the cap to the spreading of surface waves caused by the vapour jet from the opposite side of the bubble impacting on the interface with the host liquid.

Bubble growth velocity

In this study, measurements were made only on those droplets in which the actual growth plane made an angle of less than about 25° with the optimum growth plane. The maximum under-estimation of the growth velocity for any single droplet, due to this geometric effect, is about 10%. The selected droplet films were then analysed with a KONTRON digital image analyser system. The vapour outline was interactively discriminated in grey levels by a human operator. It was assumed that the vapour was cylindrically symmetrical about the projected axis from the apex of the cap to the centre of the droplet, and the volume of the solid of revolution generated by rotating the two-dimensional outline through 180° around this axis was calculated. That volume was then equated to a spherical volume and the corresponding radius r was calculated. This method is essentially identical to that of Shepherd and Sturtevant. Reproducibility of the procedure by the operator was checked and it was found to be reliable within about 10% in volume, which results in a reproducibility of about 3% in computed radius.

Figure 4 shows the measured values of r as a function of time for a typical droplet. The bubble radius reaches the initial droplet radius at about 45 μs. The growth velocity, u, can clearly be measured as a function of time for each individual droplet, averaged over the time between r measurements, and this has been

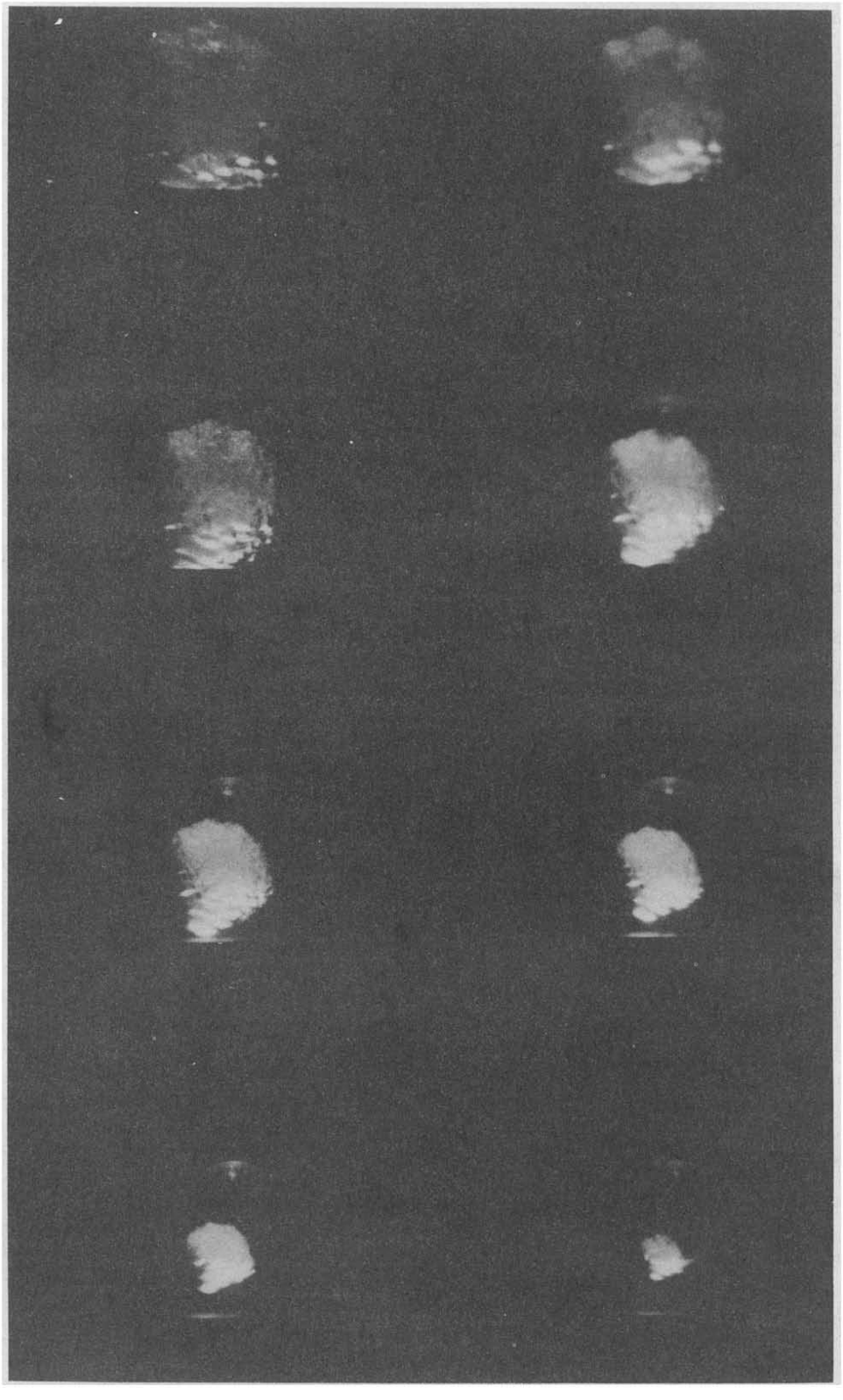

FIG. 3. The evaporation of a droplet of liquid n-butane, as recorded by the IMACON camera, at 10^5 fps. The first frame in this sequence was recorded 13 μs after nucleation. Illumination is provided by a 20/50 flash, directed from the left-hand side.

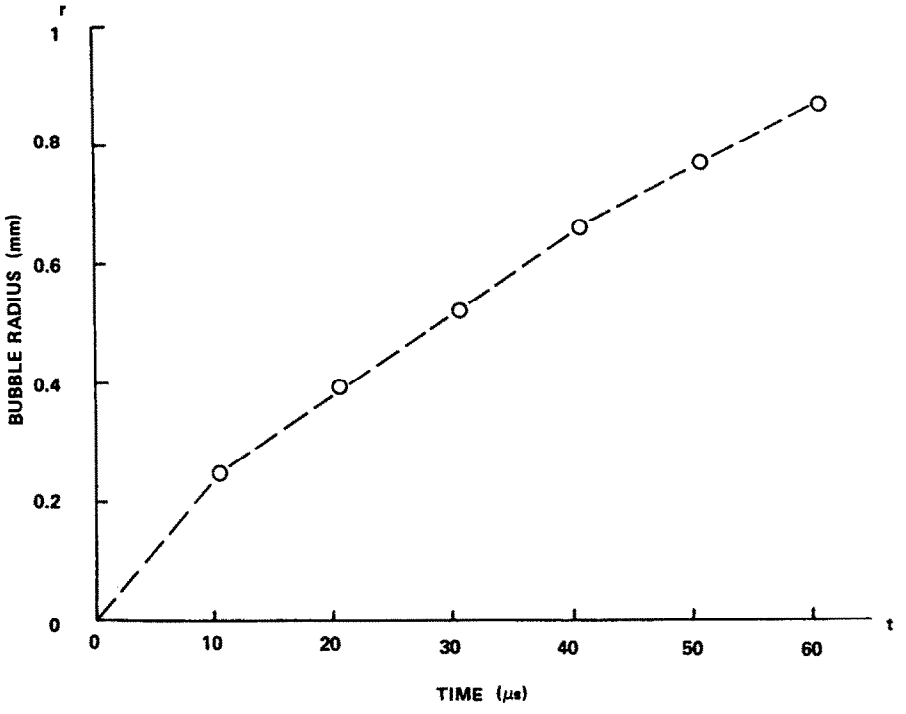

FIG. 4. Measured values of bubble radius as a function of time for a single droplet. The broken line is merely to guide the eye.

carried out for two samples of droplets filmed at 10^5 fps as will be discussed below. In each case, only the first six frames have been measured. The present technique for measuring the movement of the liquid–vapour interface is insufficiently sensitive to be meaningfully applied to droplets filmed at 5×10^5 fps. In any case, it would be preferable to measure the speed of movement of the interface directly rather than through the 'equivalent sphere' method; this would enable measurements of the movement of the interface as a function of direction from the cap, for example. This latter technique is being developed. However, at this stage it is worthwhile, nonetheless, to compare the 'equivalent sphere' results with those of Shepherd and Sturtevant and both the TRC bubble growth model and the classical theory.

Velocities were measured for two samples of droplets; both samples were filmed at 10^5 fps, one having the first frame at about 10 μs (A) the other at about 15 μs (B). Each sample contained nine droplets and the velocity values were averaged over the whole sample. The results are shown in Figs. 5(a) and (b) with their statistical errors. Three phases of growth can be clearly identified from these results: a rapid growth phase at times below about 10 μs; a phase of constant intermediate growth rate from about 10 to 45 μs; and a phase of gradually diminishing growth rate beyond about 45 μs, as the remaining volume of liquid diminishes. The average measured growth rate in the first phase is 23.8 ± 1.5 m s^{-1}, slowing down to 13.9 ± 0.5 m s^{-1} in the intermediate phase. The latter value is in very good agreement with Shepherd and Sturtevant's result.

The classical theory predicts a growth rate of about 40 m s^{-1} during the early inertially-dominated stage of growth. However, that is only expected to be sustained over a period of less than 1 μs. Then heat diffusion is expected to dominate, so that the growth rate becomes proportional to $t^{-1/2}$. These predictions are shown by the dotted curves in Figs. 5(a) and (b). In the rapid growth phase up to about 10 μs, the predicted average value of growth rate is 24 m s^{-1}, which is very close to the measured value. However, as will be shown below, the bubble growth behaviour during this phase is more complex than in the classical theory, and the observed agreement may be fortuitous. Particular attention should be paid to the data in the intermediate phase from 10 to 45 μs, since later measurements are affected by the finite size of the droplets, as remarked above. The classical theory clearly underestimates the growth rate throughout this phase. This is due, at least in part, to the non-validity of the assumption of a smooth liquid–vapour interface in the classical theory.

The predictions of the TRC bubble growth model are shown as the solid curves in Figs. 5(a) and (b), and they lie consistently above the observed values. Therefore, it is possible that fine tuning of the model might yet give good agreement with experiment, particularly in view of the fact that the complexities revealed by the study of the far-field pressure (see below) have yet to be included in the model.

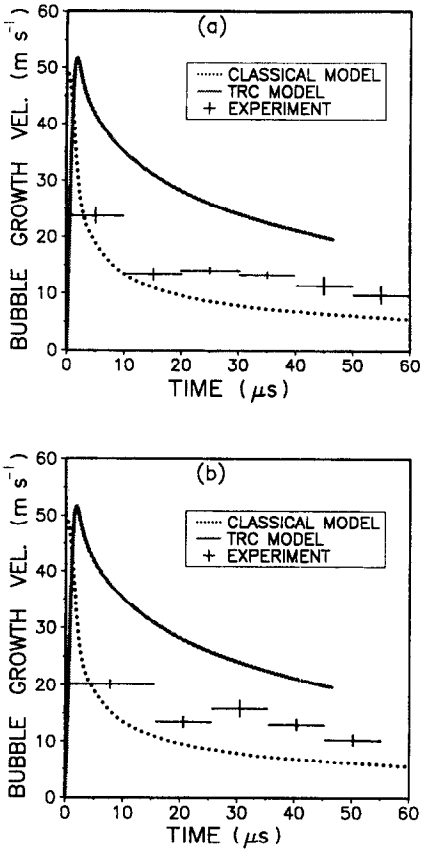

FIG. 5. The average values of the measured bubble growth rates for two samples of droplets. The vertical bar indicates the statistical error on each value, and the horizontal bar indicates the time span over which the average is measured.

PRESSURE YIELD

Measurement details

It was impossible to obtain pressure traces simultaneously with the fast illumination of the droplet, due to pick-up in the pressure measurement circuit. This effect was eliminated on the short time scale ($t < 50$ μs) by using lower-powered flashes, Hadland FH-1. These flashes have a rise time of about 20 μs before producing useful light, so the first frame was not obtained until about 30 μs after nucleation. The prominence of the cap structure, however, still allowed measurement of the nucleation position within the droplet even at that late time after nucleation. The set-up of measurement and triggering transducers is illustrated in Fig. 6. The Kistler 603B pressure measurement transducer was mounted close to the centre of the observation chamber in the geometry shown in Fig. 6 by means of a Kistler adaptor mounted through the side of the chamber. The earliest arrival of reflections from the chamber walls at the transducer is about 30 μs after the first arrival of the direct pressure pulse from the evaporating droplet. The performance of the charge amplifier was checked electronically with step inputs and inputs designed to simulate the rise of the expected pressure pulse (as per the TRC bubble growth model). Although the long-term calibration was found to be in agreement with the manufacturer's specification, the response in the first 3 μs was slightly problematical. In response to a step input waveform which gave a long-term output of height H, the output only reached $0.1H$ in the first 0.8 μs, and then increased to $0.9H$ in the next 1.2 μs. Therefore, in rough terms, an adequate response to a step input was achieved in 2.0 μs. (In view of this, the response of the 603B transducer was not checked in detail, since its rise time was given as less than 1 μs by the manufacturers). With inputs which were chosen to be representative of the rising pressure yield from the evaporating droplet, the charge amplifier gave virtually no response for about 0.8 μs, and then, over a period from about 1.0 to 3.0 μs after the start of the applied input, it yielded an output with a slope which was $10 \pm 3\%$ greater than the calibration setting dictated. This effect is corrected for in all relevant measurements below, except where actual pressure traces are displayed. Fourier analysis of the pressure traces indicated that the 330 kHz cut-off in the charge amplifier was not a serious limitation, since there were only very small relative amplitudes in the region 250–330 kHz, compared with the large amplitudes in the region about 200 kHz and below.

Approximately 180 droplets were simultaneously filmed and acoustically recorded. The majority of these had a diameter of 1.35 mm, and that is understood in the discussion below, unless explicitly stated otherwise. An example of the first 30 μs or so of the far-field pressure trace is shown in Fig. 7. The nucleation site is measured in two dimensions on the first few frames of the film sequence, using the cap as previously described. The accuracy of measurement is about $\pm 7.5°$ in the two-dimensional projection, which translates into ± 15 min in the 'clock' terms used to describe the position, as illustrated in Fig. 6. Droplets in which the actual growth plane made an angle of more than about 45° with the optimum growth plane were rejected from the analysis.

Pressure reverberation model

The suggestion of Shepherd and Sturtevant that the observed pressure oscillation on the microsecond time-scale is due to reverberation of pressure within the liquid butane has been developed into a model which can be compared with the data. This reverberation model is presented more fully in the Appendix. For the present, it is sufficient to note some of its predictions.

(a) There can only be fine structure in the pressure trace if the time derivative of the sum of the reflected amplitudes is negative and is greater in magnitude than that of the freshly-generated 'primordial' signal, assuming that the latter has a positive time derivative.

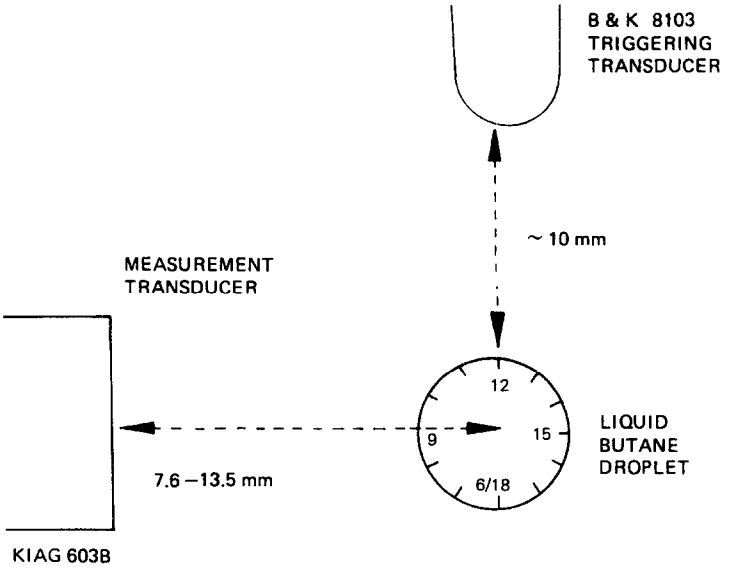

FIG. 6. Experimental set-up for pressure measurements, and illustration of the 'clock' convention for describing the nucleation position in two dimensions.

This apparently trivial observation will have significant consequences below.

(b) There should be more reverberation peaks in the pressure trace in the case where nucleation is on the side of the droplet furthest from the measurement transducer (15:00) compared with the case where nucleation is on the near side relative to the measurement transducer (9:00). This is due to the fact that, in the latter case, the growing vapour bubble eventually 'hides' the inside of the droplet from the transducer.

(c) In the 15:00 case, the first reverberation bump should occur at a time given by the time for the pressure pulse to traverse the remaining liquid droplet twice, i.e. 5.4–6 μs for a 1.35 mm diameter droplet, and 6.9–7.9 μs for a 1.77 mm diameter droplet. In each case, the ranges are given corresponding to bubble wall velocities of 10 and 40 m s^{-1}.

(d) The time between successive bumps should decrease monotonically, due to the decreasing path from bubble edge to droplet surface. The absolute values of the times between bumps is sensitive to the initial droplet diameter, the bubble wall velocity, and the speed of sound in the liquid butane.

(e) Only that part of the pressure trace before the first reverberation bump is of the primordial form due to the process of bubble growth, although its amplitude is increased to 1.8 times its primordial amplitude.

Reverberation model test

The regularity of the structure of the pressure traces from droplet to droplet is very striking. For the 1.35 mm diameter droplets, the peak height of the second bump in the trace is, on average, 3.3 ± 0.10 times that

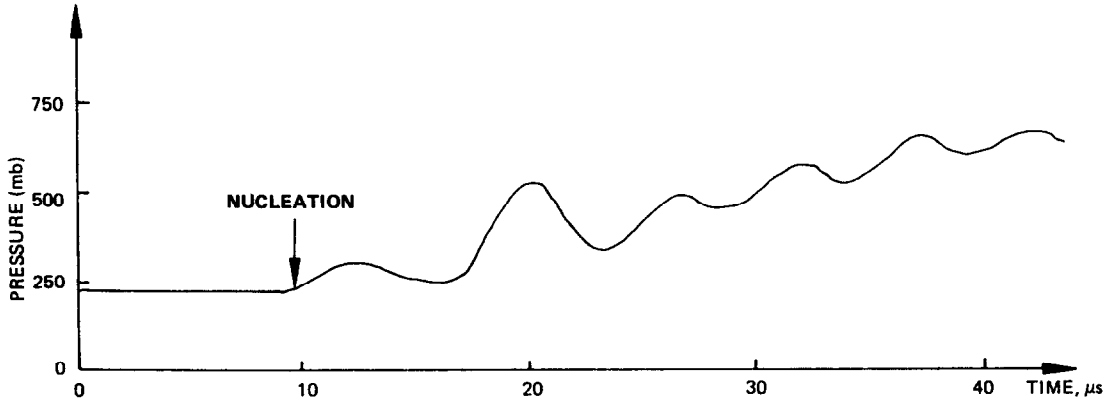

FIG. 7. A typical example of the first 30 μs or so of the pressure yield from a 1.35 mm diameter droplet of liquid n-butane vaporizing at its superheat limit temperature.

of the first bump, with a standard deviation of only 0.43, whilst the third is 0.99 ± 0.03 times the height of the second, and subsequent bumps are generally between 3 and 30% higher than the preceding bump. It is already clear that the transition from the first bump to the second is anomalous. The rate of rise of pressure to the peaks of bumps 1 and 2 in the traces will be discussed below; the rate of rise to the peak of bump 2 is always at least twice the rate to the peak of bump 1. From prediction (a) above, it therefore follows that bump 2 cannot be produced by any reverberation mechanism, neither in the increasing pressure stage, nor in its termination. Therefore, bump 2 is attributed entirely to the vapour growth phenomenon itself. This is consistent with the findings of Frost and Sturtevant, who attribute the large rate of pressure rise in the second bump to the roughening of the liquid–vapour interface.

The number of bumps in each pressure trace is shown in Fig. 8 as a function of nucleation position. It will become clear below that the first two bumps are not due to the reverberation mechanism. So, the entries at bump No. = 2 are cases where there are no measurable reverberation bumps. Near-side nucleation clearly gives fewer bumps than far-side nucleation.

The average time to the first bump and the average time separations between bumps, have been measured for two samples of droplets: 20 droplets of diameter 1.35 mm, and 9 of diameter 1.77 mm. The results are shown in Fig. 9 and in Table 1. In both samples, the average time to the first bump is well below the expected time due to the reverberation mechanism, and the spread of the individual values of δ_1 in each sample is large, leading to a large error in $\langle \delta_1 \rangle$ in each case. From $\langle \delta_{23} \rangle$ onwards, the errors are relatively small, reflecting the small spread of the underlying distributions. In the case of the smaller droplets, the time between bumps does clearly fall monotonically from $\langle \delta_{12} \rangle$ onwards, up to $\langle \delta_{67} \rangle$. The same trend is seen in the larger droplets, but only from $\langle \delta_{23} \rangle$ onwards. The ratios of $\langle \delta \rangle$ values between the two droplet samples are also given in Table 1, and they show that, from $\langle \delta_{23} \rangle$ onwards, the data are consistent with a constant ratio of about 1.4. However, the $\langle \delta_1 \rangle$ values are identical within experimental error, and the $\langle \delta_{12} \rangle$ values give a ratio which is intermediate between the two cases above. These data support the contention that reverberation in the traces only really begins to show through after the second peak has been reached. This is to be expected, since the high pressures reached at that point dwarf the reverberation of primordial pressures from earlier times.

In view of the above, only $\langle \delta_{23} \rangle$, $\langle \delta_{34} \rangle$, etc., have been compared with reverberation calculations below. Guided by the above results, it was assumed that the primordial pressure had a two-stage behaviour, rising linearly for the first 2.5 μs, then becoming flat before rising linearly again from 7 to 10 μs, and again becoming flat. A simple ray-tracing program incorporated the varying bubble wall velocity, as discussed above; u was taken to be 25 m s^{-1} for the first 10 μs, and 14 m s^{-1} thereafter. It was found that the speed of sound in liquid butane, c, had to be increased from 426 to 550 m s^{-1} in order to reproduce both the trend of the observed data and the individual $\langle \delta \rangle$ values (within about 1 μs). The most important observation is that the reverberation calculations reproduce the experimentally observed ratios of $\langle \delta \rangle$ values between the two droplet samples, as shown in Table 1. To a first approximation, c cancels out in these ratios. Therefore, this test is valid even in the case where there is considerable uncertainty in c. The above experimental observation strongly supports the reverberation mechanism. It is concluded that reverberation is the dominant source of the oscillations in the observed pressure traces after about 10–13 μs.

The first six microseconds

As was noted above, there is a wide variation in the time at which the peak of the first bump occurs in the pressure trace. In fact, it shows a very strong dependence on the position of the nucleation site relative to the measurement transducer, as shown in Fig. 10: for near-side nucleation sites, the peak of bump 1 occurs at about 5.5 μs, whereas, for far-side nucleation sites, it occurs at about 2.5 μs, typically. Closer examination of the very early pressure field showed the following additional features.

(a) Far-side nucleation cases showed a subsidiary bump in the trough between bumps 1 and 2 which are identified in the coarser-scale pressure traces, as illustrated in Fig. 11(a). These trough bumps are measured to occur at 5.5 μs, on average.

(b) Near-side nucleation cases showed a distinct break in the rate of pressure rise, to a lower value, at a time about half-way between zero and the peak. This is illustrated in Fig. 11(b). The break is measured to occur, on average, at 2.6 μs after nucleation.

The above features have been entered in Fig. 10, assuming the rise-breaks to be somehow related to the same phenomenon as that which gives rise to early peaks of bump 1, and the trough bumps to be similarly related to late peaks of bump 1. From Fig. 10, this association seems quite strong, and it is concluded that there are two constant features in the data, which appear in a different context depending on the nucleation site.

A self-consistent model for the above effects can be constructed by invoking the visual observation by Frost [7, 15] that, when the (originally smooth) growing bubble breaks through the droplet edge, heterogeneous nucleation takes place near the intersection of the bubble surface with the droplet edge and the ethylene glycol, and boiling spreads outwards along the surface of the droplet: in the near-side nucleation case, it is assumed that the initial pressure rise levels off at about 2.5 μs or so for some reason

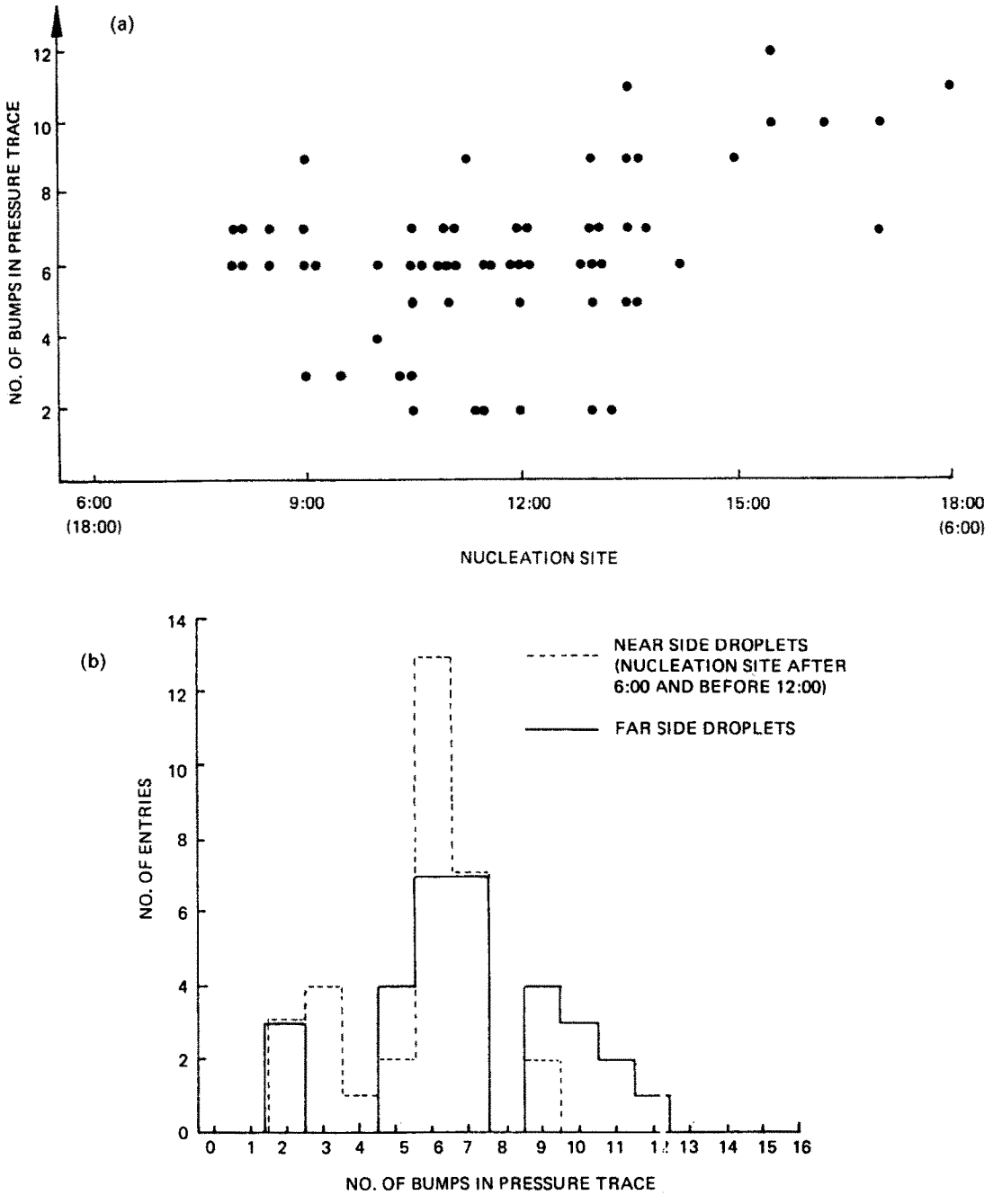

FIG. 8. (a) Number of bumps in the pressure trace as a function of nucleation site with respect to the transducer. (b) Projection of (a) for two categories, namely near-side droplets (dashed histogram), and far-side droplets (solid histogram).

which can be left open for the time being. Very shortly after this, the above heterogeneous nucleation takes place and the observed pressure rises as more bubble growth ensues, the pressure from which also levels off after a further 2.5 μs or so. In the far-side case, the pressure yield due to heterogeneous nucleation is postulated to be 'hidden' from the transducer due to the heterogeneous nucleation taking place at points slightly removed from the intersection of the droplet edge with the vapour bubble, as illustrated in Fig. 12. This pressure is then almost completely reflected at the liquid butane–vapour interface. In the case of the trough bumps at about 5.5 μs in the far-side case, this provides an explanation for the slight rise in observed pressure leading to the bump; the bubbles arising form the heterogeneous nucleation sites are eventually large enough that the initial bubble does not obstruct the path between them and the transducer.

Similar behaviour is observed in general for the 1.77 mm droplets. In particular, it is observed that there is

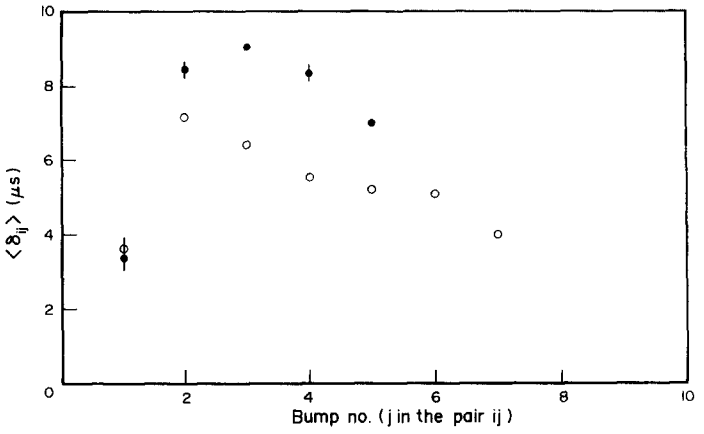

FIG. 9. Average values of δ_{ij}, with statistical errors which, in most cases, are smaller than the marker size.

Table 1. Values of $\langle \delta \rangle$ observed experimentally, and the ratios between the two droplet samples, from both experiment and reverberation model calculations

	Droplet size		Ratios	
	1.35 mm	1.77 mm	Experiment	Model
$\langle \delta_1 \rangle$	3.614±0.236	3.389±0.333	0.94±0.11	
$\langle \delta_{12} \rangle$	7.161±0.151	8.450±0.181	1.18±0.04	
$\langle \delta_{23} \rangle$	6.423±0.032	9.083±0.123	1.41±0.02	1.37
$\langle \delta_{34} \rangle$	5.581±0.055	8.388±0.226	1.50±0.04	1.36
$\langle \delta_{45} \rangle$	5.244±0.090	7.072±0.170	1.35±0.04	1.37
$\langle \delta_{56} \rangle$	5.128±0.056			
$\langle \delta_{67} \rangle$	4.047±0.089			

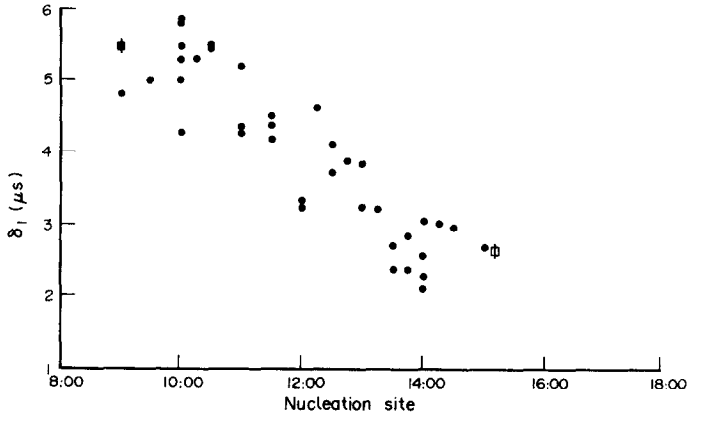

FIG. 10. Time to bump 1 as a function of nucleation site (●). The error on each measured time is smaller than the marker size. The square markers indicate the average time to the 'rise breaks' in the 9:00 case (□) and the 'trough bumps' in the 15:00 case (■), with their errors. (See text.)

a similar fall in pressure after about 5.5 μs, into the trough between bumps 1 and 2. In view of the results discussed above, this implies that bump 1 is not caused by reverberation, and it must be attributed to bubble growth itself. It is concluded that there is a characteristic time of about 2.5 μs for pressure rise consequent upon nucleation and smooth bubble growth at T_{SL}.

Testing the TRC bubble growth model

The TRC bubble growth model has only been developed for the case of a liquid of infinite extent and uniform properties except insofar as temperature gradients over small regions can be imposed, and bubble growth can be restricted to spherical domains. It is clear from the above discussion that there are many difficulties in testing such a model quantitatively with

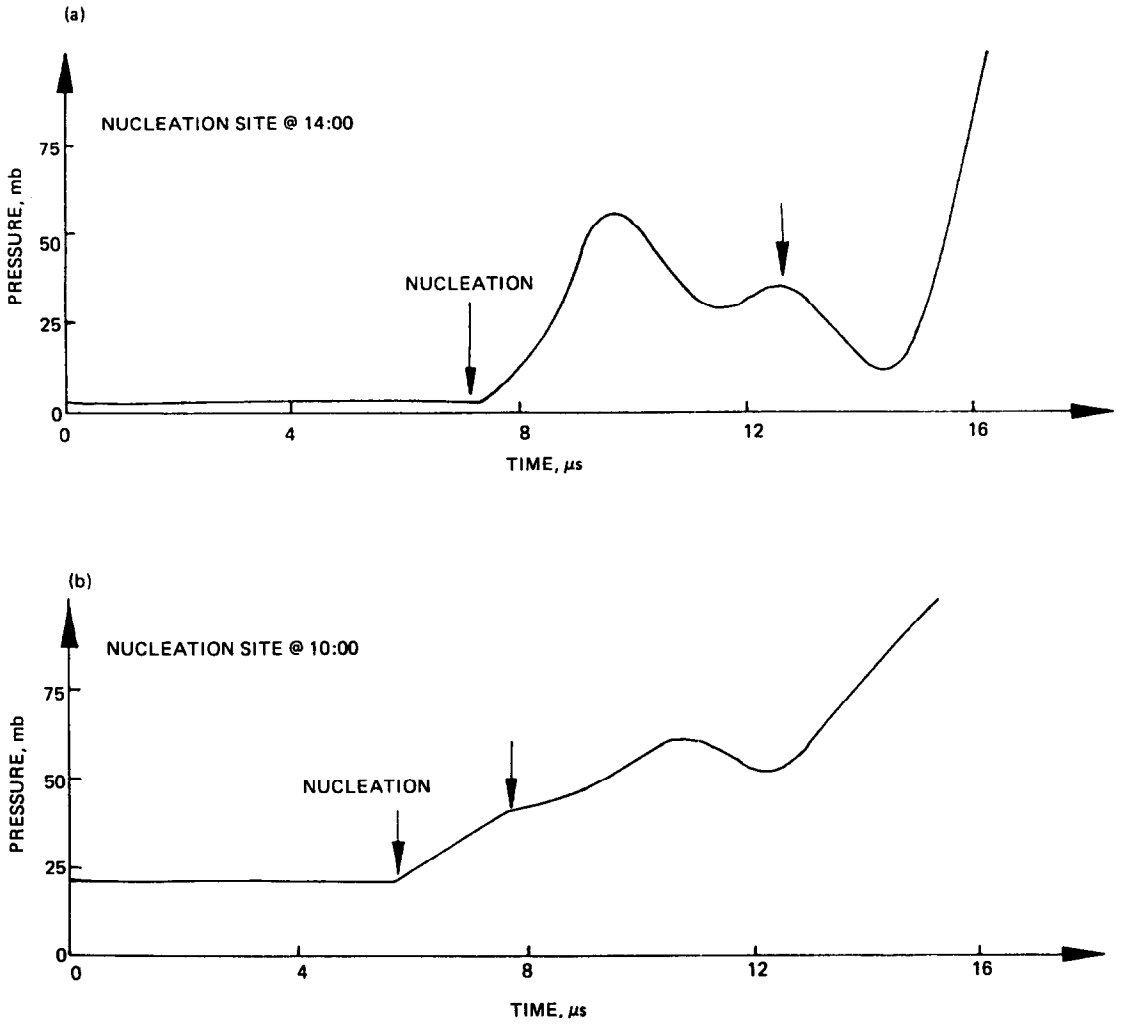

FIG. 11. (a) An illustration of the bump in the trough in cases where nucleation is near to 15:00. (b) An illustration of the break in the slope to bump 1 in cases where nucleation is near to 9:00.

a liquid sphere of only about 1 mm in diameter. However, it has been demonstrated in the previous sections that the bubble growth process itself yields two distinct phases of pressure yield: the first gives a peak about 2–5.5 μs after nucleation and the second gives a much larger peak at about 10–15 μs after nucleation. This two-stage pressure yield is not predicted by the TRC model, but the model implicitly assumes that, whatever the process which causes the necessary roughening of the vapour–liquid interface, it is driven by a large pre-instability evaporation rate. This might have been expected to occur at very early times, much less than 1 μs, during the short-lived inertially-dominated phase predicted by the classical bubble growth theory. However, Frost and Sturtevant [6, 7] have demonstrated that the instability is 'triggered' at a much later time, about 7 μs or so for 1 bar ambient pressure, by the bubble bursting out of the liquid drop, and there is much supporting evidence for that in the analysis presented here. Frost and Sturtevant also show that there is probably a strong influence of pre-instability evaporation rate on whether a given liquid is actually susceptible to the instability.

Due to the reverberation process, it is only meaningful to compare the early rate of rise of pressure, dp/dt, between theory and experiment. This has been measured for 39 droplets during the rise to the peaks of both the first and second bumps in the pressure traces. The results have been correlated with nucleation site and are shown in Fig. 13 for the first bump. There is a strong dependence on the position of the nucleation site relative to the measuring transducer, which was 13.5 mm from the droplets in this test. The dependence may be due entirely to the acoustic lens effect of the butane–glycol interface, but no attempt has been made to calculate that effect. The same trend is observed for the bump 2 data, over the range 18–77 mbar μs^{-1}, which is to be compared with the bump 1 data range of 7–33 mbar μs^{-1}.

The TRC model can yield large variations in dp/dt

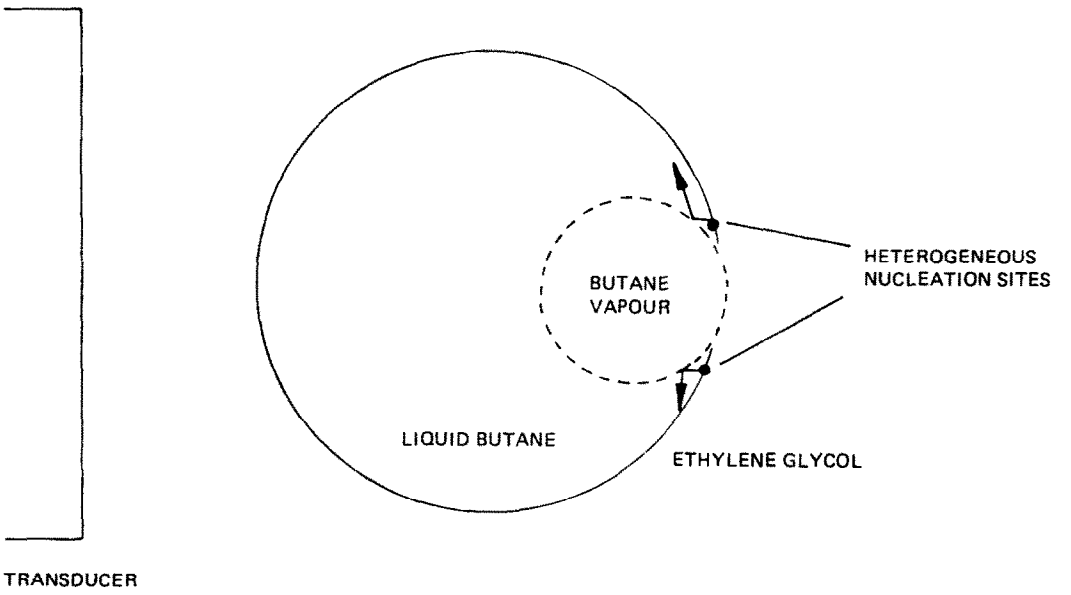

FIG. 12. Mechanism by which, in the 15:00 homogeneous nucleation case, new heterogeneous nucleation sites may not be 'seen' by the transducer in the early stages of their growth; almost complete reflection occurs at the interface between the liquid butane and its vapour.

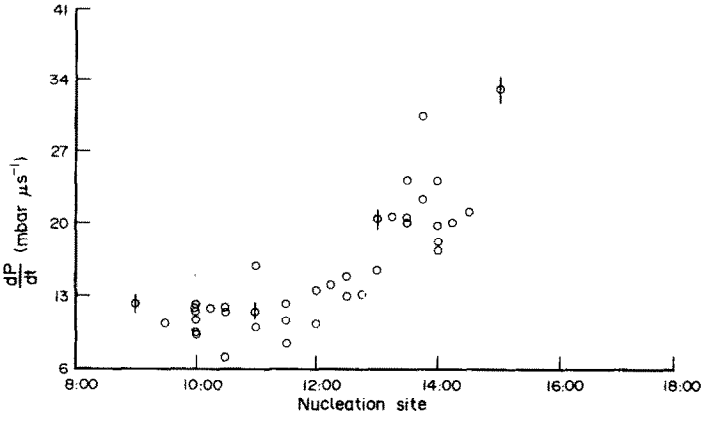

FIG. 13. The steepest rise in $P(t)$ (for each pressure trace) on the rise to bump 1, as a function of nucleation position. Only a few entries have representative error bars shown.

even if only the nucleation position and the temperature distribution in the droplet are varied. In the case where nucleation occurs at the droplet wall, the model predicts a rise of 181 mbar μs^{-1} for a droplet of constant temperature, but only 71 mbar μs^{-1} if it is assumed that the droplet temperature falls by 55°C from the edge to the centre. In both of these calculations, the model results have been scaled up by the acoustic transmission coefficient, so they can be compared directly with the data. In view of the range of bump 2 data above, it is clear that there is some overlap between the TRC model and the experimental data. However, any further comparison with the present experimental data would require some investigation of the acoustic lensing effect in the system.

The far-field pressure predicted by the classical theory is about two orders of magnitude less than that observed in these experiments. Shepherd and Sturtevant have shown that this is due to the low rate of mass transfer in the classical theory, compared with that which can be inferred from their experimental measurements of both the far-field pressure and the evaporative surface of the bubble. This experiment has confirmed their data and has shown that the pressure yield, even in the most violent phase of the vaporization, may be described by the TRC bubble growth model within a factor of two or so.

CONCLUSIONS

The vaporization of a liquid raised to its superheat limit temperature has been filmed at speeds about 100

times faster than in any previous experiments, opening up new possibilities in the study of this phenomenon. The analysis of the film to date reveals that the average rate of bubble growth in the first 10 μs is 24 m s^{-1}, and confirms the finding of Shepherd and Sturtevant [4] that the rate of bubble growth is about 14 m s^{-1} from about 10 to 45 μs after nucleation. The classical theory of Prosperetti and Plesset [8] is consistent with the measurement in the first 10 μs. However, in the 10–45 μs period, it predicts growth rates which are as low as half of the measured values. The TRC bubble growth model [12] gives predictions which are about 50% larger than the experimentally observed values. The fast rate of growth of the bubbles is attributed to a roughening of the interface between the liquid and the vapour, as first reported by Shepherd and Sturtevant and which is confirmed here.

Far-field pressure measurement is complicated by the multiple reflection of the primordial pressure within the butane droplet; this effect has been conclusively demonstrated to occur by observation of several specifically predicted consequences. Nonetheless, structures in the observed pressure traces at times less than about 13 μs are dominantly due to the bubble growth process itself, rather than reverberation. A two-stage increase of pressure is evident during this period, with the second being more rapid by a considerable margin. The TRC bubble growth model, with parameters as presented in ref. [12], predicts a range of values for the rate of rise of far-field pressure which overlaps with the experimentally observed range in the second stage of the early pressure rise. The experimental measurements of this quantity display a marked dependence upon the position of the nucleation site relative to the measurement transducer.

Further details of both the photographic data and the far-field pressure have been studied extensively, and several of these are consistent with the visual observation by Frost [7, 15] that the instability which roughens the bubble surface is 'triggered' by the growing bubble bursting through the droplet surface.

Acknowledgements—We are indebted to many people at Thornton Research Centre for their contributions to this experiment at various stages. In particular, we wish to thank Mr R. P. Wilson for his assistance with photographic aspects of the work, Dr K. Reading and Miss K. G. Hurst for their development of the image analysis algorithm for measurement of bubble radius, Mr M. J. M. IJpelaar for carrying out calculations of the TRC model for our specific experimental conditions and Dr V. T. Nguyen for many wide-ranging discussions concerning both experimental and theoretical aspects of this phenomenon. This paper was presented at the 25th U.S. National Heat Transfer Conference, Houston, Texas, U.S.A., July 1988.

REFERENCES

1. R. C. Reid, Rapid phase transitions from liquid to vapor, *Adv. Chem. Engng* **12,** 105 (1983).
2. M. Blander and J. L. Katz, Bubble nucleation in liquids, *A.I.Ch.E. Jl* **21,** 833 (1975).
3. C. T. Avedisian, The homogeneous nucleation limits of liquids, *J. Phys. Chem. Ref. Data* **14,** 695 (1985).
4. J. E. Shepherd and B. Sturtevant, Rapid evaporation at the superheat limit, *J. Fluid Mech.* **121,** 379 (1982).
5. C. T. Avedisian, An experimental study of high-pressure bubble growth within multicomponent liquid droplets levitated in a flowing stream of another immiscible liquid, *Proc. R. Soc. A* **409,** 271 (1987).
6. D. Frost and B. Sturtevant, Effects of ambient pressure on the instability of a liquid boiling explosively at the superheat limit, *J. Heat Transfer* **108,** 418 (1986).
7. D. L. Frost, Dynamics of explosive boiling of a droplet, *Physics Fluids* **31,** 2554 (1988).
8. A. Prosperetti and M. Plesset, Vapour-bubble growth in a superheated liquid, *J. Fluid Mech.* **85,** 349 (1978).
9. L. D. Landau, On the theory of slow combustion, *Acta Phys.-chim. URSS* **19,** 77 (1944).
10. A. Prosperetti and M. Plesset, The stability of an evaporating liquid surface, *Physics Fluids* **27,** 1590 (1984).
11. F. J. Higuera, The hydrodynamic stability of an evaporating liquid, *Physics Fluids* **30,** 679 (1987).
12. V. T. Nguyen, R. M. Furzeland and M. J. M. IJpelaar, Rapid evaporation at the superheat limit, *Int. J. Heat Mass Transfer* **31,** 1687 (1988).
13. G. R. Moore, Vaporization of superheated drops in liquids, *A.I.Ch.E. Jl* **5,** 458 (1959).
14. V. P. Skripov, *Metastable Liquids.* Wiley, New York (1974).
15. D. L. Frost, Effects of ambient pressure on the instability of a liquid boiling explosively at the superheat limit, Ph.D. Thesis, California Institute of Technology (1985).
16. R. C. Weast (Editor), *CRC Handbook of Chemistry and Physics.* CRC Press, Boca Raton, Florida (1984).
17. W. M. Haynes and R. D. Goodwin, Thermophysical properties of normal butane from 135 to 700 K at pressures to 70 MPa, *NBS Monogr.* 169 (1982).
18. R. Niepmann, Thermodynamic properties of propane and n-butane—2. Speeds of sound in the liquid up to 60 MPa, *J. Chem. Thermodyn.* **16,** 851 (1984).

APPENDIX: A MATHEMATICAL MODEL OF THE REVERBERATION PROCESS

Pressure reverberation within the liquid butane is to be expected, given the reflection coefficients at the relevant interfaces: 0.771 for liquid butane–ethylene glycol and −0.996 for liquid butane–butane vapour. The relevant properties of butane and ethylene glycol are given in Table A1. The simplest basis for a model is to assume that the vapour bubble nucleates adjacent to one side of the droplet—this defines the origin of the one-dimensional axis system—and the pressure is measured outside the droplet diametrically opposite the point of nucleation. The first of these conditions is nearly always found to be the case, experimentally. The second, however, is only true in a small number of cases (the 15:00 cases in the main text). The bubble wall position is given by $x = ut$. The outer wall of the droplet remains fixed with respect to the origin so that the region of liquid butane between the vapour wall and droplet wall decreases with time. The photographic evidence lends credence to this assumption, since it is indeed observed that the interface between the liquid n-butane and the ethylene glycol moves very slowly compared to that between the liquid n-butane and its growing vapour. The model developed here considers only one-dimensional pressure propagation and assumes the boundary between the liquid butane and the ethylene glycol to be planar.

A convenient representation of the process is given in Fig. A1. Constant values of time are denoted as upper case, T, with subscripts. Time T_1 is defined as the earliest moment at which a pressure signal from the nucleating vapour bubble can reach the droplet boundary D, and is simply D/c. The proportion of the pressure pulse that is reflected at T_1 returns

Table A1. Parameters for reverberation calculations

	Ethylene glycol $C_2H_6O_2$	Liquid butane C_4H_{10}	Butane vapour
Density (105°C, 1 bar), kg m^{-3}	1050 [16]	466 [17]	1.89 [17]
Sound velocity (105°C, 1 bar), m s^{-1}	1463 [16]	426 [18]	237 [17]
Acoustic impedance, kg m^{-2} s^{-1}	1.54×10^6	1.99×10^5	4.47×10^2

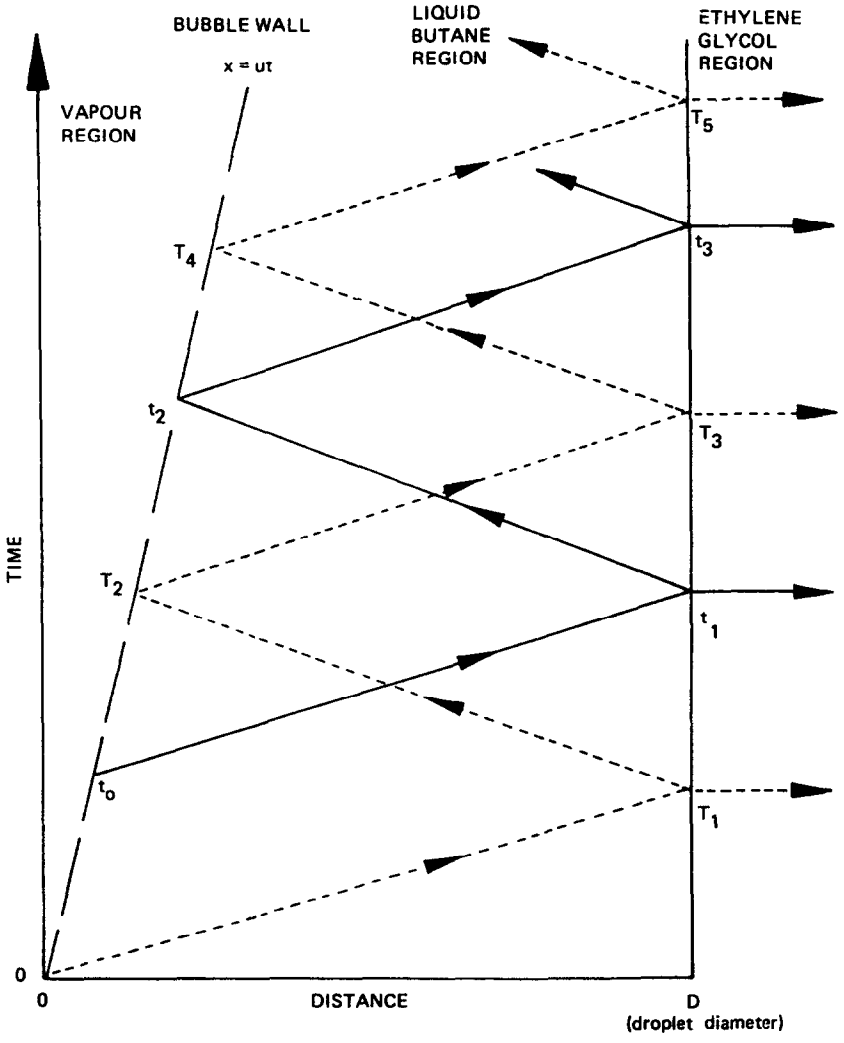

FIG. A1. One-dimensional model of pressure wave reverberation within liquid butane droplet.

to the vapour wall at time T_2 and eventually returns to the droplet boundary again at time T_3. As a consequence, the signal that propagates into the ethylene glycol at a time t_1 such that $T_3 > t_1 \geqslant T_1$ exhibits no reverberation effects: it is simply the original pressure pulse from the bubble wall, changed in magnitude by the transmission coefficient and delayed by the transit time across the droplet. Only after time T_3 will the pressure pulse contain reflected contributions. Any pressure pulse that emerges from the droplet at time t_3 (i.e. after T_3 but before T_5) will be a superposition of two signals: that coming directly through the butane from the expanding vapour wall (i.e. generated at a time $t_2 > T_2$) and that which was generated earlier in time and has already been internally reflected once from the droplet wall. In general, since the reflected signal must now have negative amplitude, the observed rate of increase of pressure will be reduced from that due to the freshly-generated signal. The observed pressure will start to fall only if the pressure generated at the bubble wall at time $t_0 < T_1$ was rising at a rate faster than that of the freshly-generated signal multiplied by the inverse of 0.771×0.996. It is possible to define subsequent times T_5, T_7 and so on, which demarcate time zones in which the outgoing pressure pulses may contain 3, 4 or more superimposed pressure contributions. To generalize, any time between T_{2n+1} and T_{2n+3} at the droplet boundary is written as t_{2n+1}, and signifies that the number of reflection contributions to the transmitted signal is n. Also, any time between T_{2n} and T_{2n+2} at the vapour wall is denoted t_{2n}.

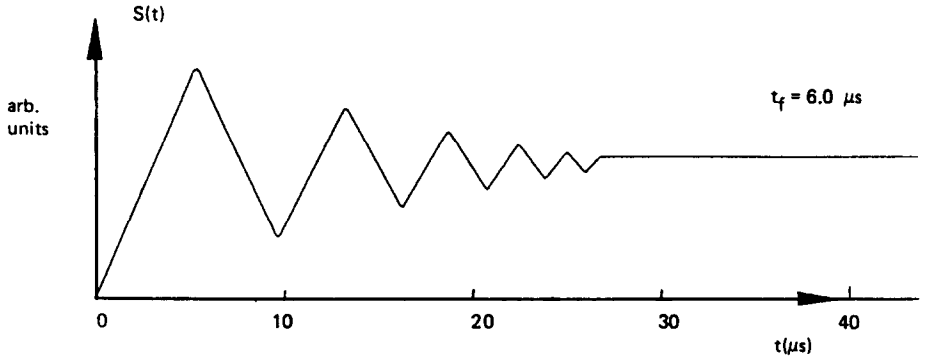

FIG. A2. The pressure form resulting from reverberation, with $t_f = 6$m μs and $u = 40$ m s^{-1}.

This model has been coded in FORTRAN for comparison with the data. The following relationships are used:

$$t_{2n} = [(c-u)/(c+u)]t_{2n-2} + 2D/(c+u) \quad \text{(A1)}$$

$$t_{2n+1} = [(c-u)/c]t_{2n} + D/c. \quad \text{(A2)}$$

The primordial pressure, $q(t)$, varies with time, so the pressure arriving at the droplet boundary at a particular time t_{2n+1} is a superposition of contributions generated at time t_{2n}, t_{2n-2} and so on. The total number of possible reflected contributions, i, is limited by n, i.e. $i \leqslant n$. It is simple to show that the time-dependent signal, $s(t_{2n+1})$, emerging from the droplet boundary, D, at time t_{2n+1} is

$$s(t_{2n+1}) = T_D \sum_{i=0}^{n} (R_0 R_D)^i q(t_{2n-2i}). \quad \text{(A3)}$$

In this summation, the $i = 0$ term represents the fresh primordial contribution, i.e. having undergone no reflections. Several calculations of $s(t)$ have been carried out with different input forms of $q(t)$. The TRC bubble growth model [12] suggests that $q(t)$ rises linearly and then becomes flat at time t_f. Figure A2 shows the results of the calculation of equation (A3) for $t_f = 6$ μs, with $u = 40$ m s^{-1}.

ETUDE EXPERIMENTALE DE LA FORMATION DE VAPEUR A LA TEMPERATURE LIMITE DE SURCHAUFFE

Résumé—La vaporisation du n-butane liquide à la température limite de surchauffe est filmée à des vitesses atteignant 5×10^5 vues par seconde et on étudie le champ lointain de pression qui est associé. On mesure des vitesses de croissance de bulles de 25 m s^{-1} et on compare avec des modèles théoriques et des données expérimentales antérieures. Le champ de pression lointain est distordu par des réflexions multiples dans des gouttes de butane, bien que ceci n'explique pas toute la structure, dans les 13 premières μs, des pressions enregistrées; en particulier, la croissance des bulles devient très dramatique après environ 7 μs. D'autres détails des traces de pression peuvent être compris à partir du comportement des bulles.

EXPERIMENTELLE UNTERSUCHUNG DES BLASENWACHSTUMS BEI MAXIMALER ÜBERHITZUNGSTEMPERATUR

Zusammenfassung—Die Verdampfung von flüssigem n-Butan bei seiner maximalen Überhitzungstemperatur wurde mit 5×10^5 Bildern pro Sekunde gefilmt. Der zugehörige Druck im weiteren Umfeld der Blase wurde untersucht. Es wurden Blasenwachstumsgeschwindigkeiten bis zu 25 m s^{-1} gemessen. Diese wurden mit theoretischen Modellen und früheren experimentellen Ergebnissen verglichen. Das Druckfeld wird durch mehrfache Reflexionen im Butantropfen gestört; dies erklärt aber noch nicht die gesamte Struktur des zeitlichen Druckverlaufs in den ersten 13 μs. Insbesondere wird das Blasenwachstum nach ungefähr 7 μs geradezu dramatisch. Verschiedene andere Details des Druckverlaufs können auf Grund des Blasenverhaltens verstanden werden.

ЭКСПЕРИМЕНТАЛЬНОЕ ИССЛЕДОВАНИЕ ПАРООБРАЗОВАНИЯ ПРИ ПРЕДЕЛЬНОЙ ТЕМПЕРАТУРЕ ПЕРЕГРЕВА

Аннотация—Со скоростью до 5×10^5 кадров в секунду фотографируется процесс парообразования жидкого н-бутана при предельной температуре перегрева и исследуется связанное с испарением давление в дальнем поле. Измеряются скорости роста пузырьков до 25 м с$^{-1}$, и проводится их сравнение с теоретическими моделями и имеющимися экспериментальными данными. Давление в дальнем поле искажается множественными отражениями в капле бутана, но этот факт не объясняет всей структуры давлений, записанных за первые 13 мкс, в частности, рост пузырьков претерпевает значительные изменения приблизительно через 7 мкс. Поведение пузырьков может объяснить различные другие детали в следе давления.